Behzad Razavi

The Design of an Equalizer—Part One

Equalizers are widely used in broadband wireline systems. At high data rates, the imperfections of the medium through which the signal travels (the "channel") become more critical, making equalization an essential function in receivers (Rxs).

In this two-part article, we study the transistor-level design of a high-speed equalizer in 28-nm CMOS technology. The first part describes channel modeling and linear equalizer design. The second part deals with decision-feedback equalizers (DFEs). We target the following performance:

- Data format: nonreturn to zero
- Data rate = 56 Gb/s
- Channel loss at 28 GHz = 20 dB
- Input differential swing = 800 mV$_{pp}$
- Bit error rate (BER) <10^{-12}
- Power consumption = 10 mW
- V_{DD} = 1 V.

It is customary to specify the channel loss at the "Nyquist frequency," f_{Nyq}, i.e., the frequency equal to half of the data rate. The reader is referred to several background articles [1]–[3] and the vast literature on the subject [4]–[17]. The simulations are carried out with $V_{DD} = 1\,V - 5\%$ in the slow-slow corner of the process and at $T = 75\,°C$.

General Considerations

The purpose of equalization in an Rx is to compensate for channel nonidealities and reproduce the transmitted data with a low error rate. The design must

therefore assume certain characteristics for the channel. We employ a "scalable" model that reflects the physical loss mechanisms in copper media [1]. Shown in Figure 1(a) is one section of the model, with its horizontal and vertical branches representing frequency-dependent copper and dielectric losses, respectively [1]. The component values are obtained by fitting the circuit's magnitude and phase responses to

those computed by electromagnetic field simulations of a 50-Ω channel. Cascading 12 such sections yields the loss profile depicted in Figure 1(b) and a value of 21 dB at 28 GHz. Note that the line is driven by a 50-Ω source and is terminated with a 50-Ω load.

In addition to loss, copper media can also suffer from impedance discontinuities. For example, a connector attaching a cable to a line card

(a)

(b)
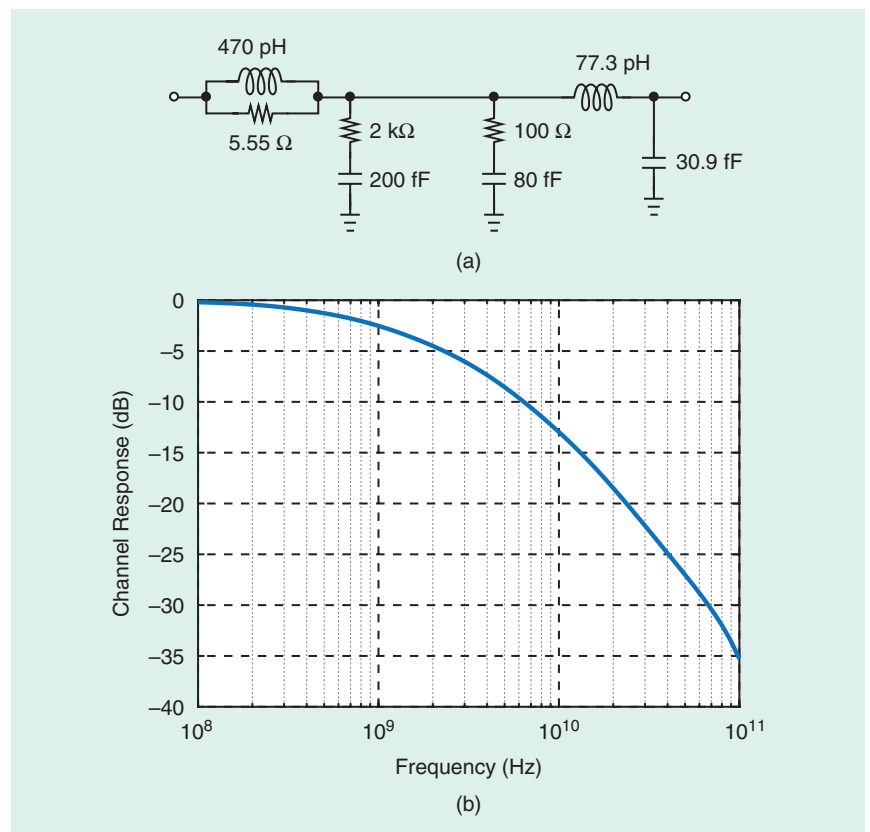
FIGURE 1: (a) One section of a scalable channel model and (b) the loss profile for 12 cascaded sections.

may exhibit an impedance that has a real component different from 50 Ω as well as a finite imaginary value. As a result, the frequency response experiences a deep notch, an effect that can be compensated by a DFE but not by a linear equalizer.

Analog equalization in Rxs is realized by a continuous-time linear equalizer (CTLE) and a DFE [Figure 2(a)]. The CTLE ideally "inverts" the channel, i.e., it provides the inverse of the channel's frequency response so that the product of their transfer functions has a relatively flat magnitude up to the Nyquist frequency [Figure 2(b)]. We say that the CTLE "boosts" the high-frequency com-ponents of the received data. In practice, however, various tradeoffs in CTLE design allow only partial flattening of the response, thereby requiring that the DFE perform further equalization.

The significance of the Nyquist frequency, f_{Nyq}, is better appreciated by examining the channel response in the time domain. Consider a random sequence of ones and zeros arriving at a rate of r_b bits per second, i.e., with a bit period of $1/r_b = T_b$. As depicted in Figure 3(a), such a sequence can follow a 0–1–0–1 pattern for some time, e.g., from 5.3 to 5.4 ns, which we consider a periodic signal having a fundamen-tal frequency of $(1/r_b)/2 = f_{Nyq}$. This periodic segment experiences the greatest degradation in the channel, as illustrated by the differential waveforms in Figure 3(b) for a loss of 12 dB at f_{Nyq}. But we also recognize that the worst case occurs for the first transition, which arrives after 5.25 ns, i.e., after the channel has "relaxed." As the periodic segment proceeds, the output reaches the steady state and a greater swing.

Basic CTLE Stage

The most common approach to creating a boost at high frequencies incorporates resistive and capacitive degeneration in a differential
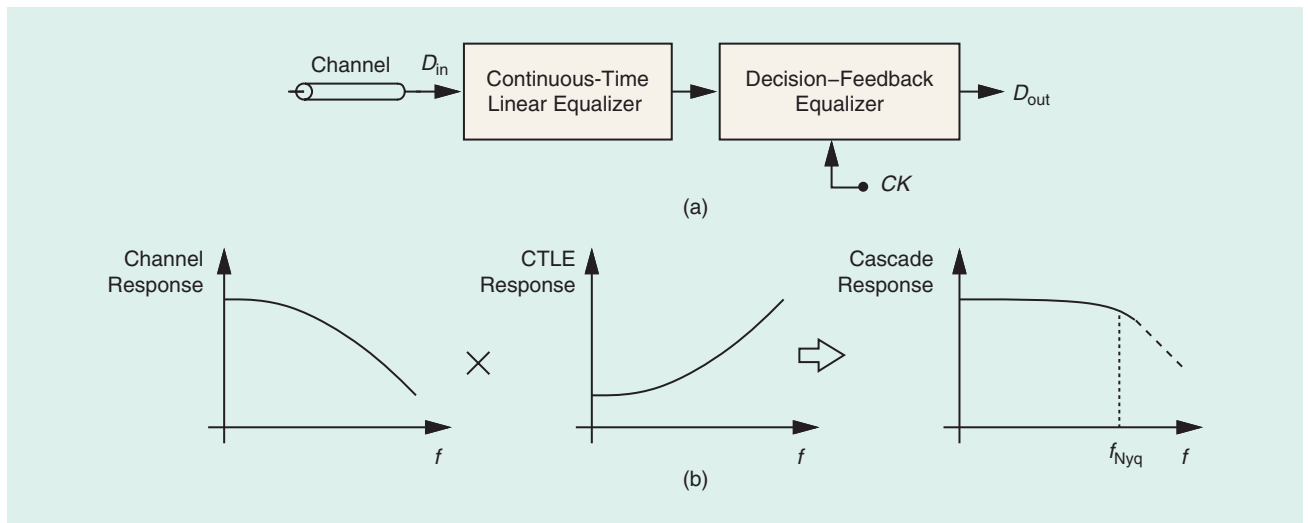
FIGURE 2: (a) A typical equalizer architecture and (b) an illustration of its overall frequency response.
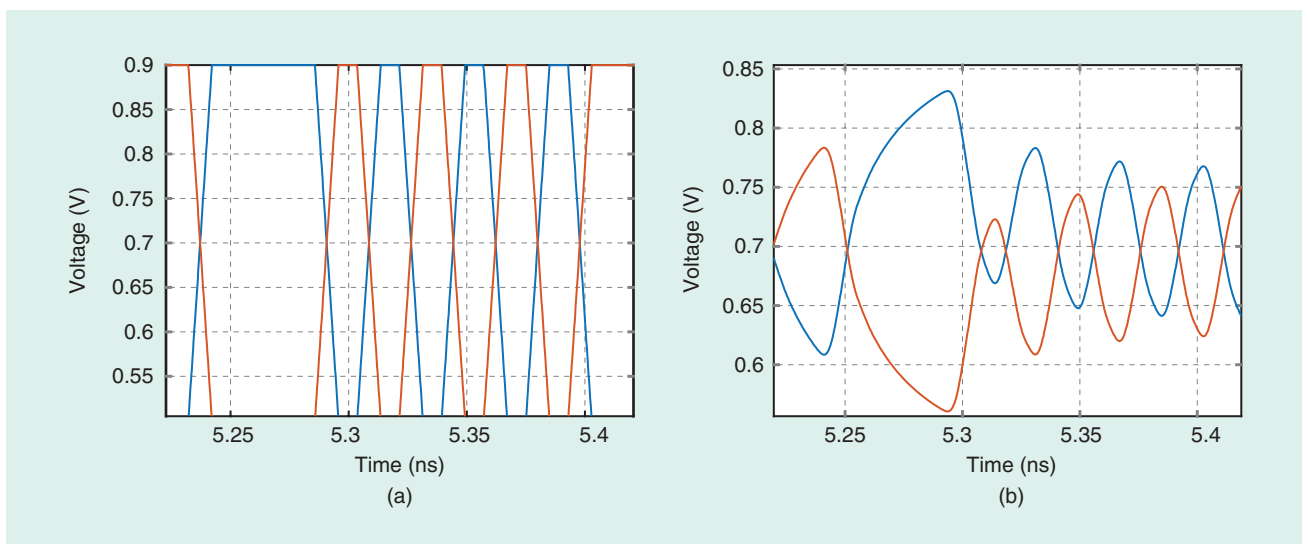
FIGURE 3: (a) The input and (b) output waveforms of a lossy channel.

pair, as shown in Figure 4(a). It can be readily proved that the circuit's transfer function, $H(s) = V_{out}/V_{in}$, is given by

$$H(s) = \frac{-g_m R_D (R_S C_S s + 1)}{R_S C_S s + 1 + g_m R_S/2}, \quad (1)$$

where g_m denotes the transconductance of M_1 and M_2 and channel-length modulation is neglected. The stage exhibits a zero and a pole, respectively:

$$|\omega_z| = \frac{1}{R_S C_S} \quad (2)$$

$$|\omega_p| = \frac{1 + g_m R_S/2}{R_S C_S}, \quad (3)$$

and the magnitude of its response varies from $g_m R_D/(1 + g_m R_S/2)$ at low frequencies to $g_m R_D$ at high frequencies [Figure 4(b)]. The circuit thus provides a boost factor of $1 + g_m R_S/2$. Note that the zero and pole frequencies are separated by the same factor.

The CTLE stage of Figure 4(a) merits two remarks. First, the boost factor trades with the low-frequency gain (also called the *dc gain*), $g_m R_D/(1 + g_m R_S/2)$. We wish to maintain this gain around unity so that the received data swings are not attenuated. With low supply voltages and channel-length modulation, the boost factor typically does not exceed 6 dB. Second, we surmise that ω_p should be placed roughly around the Nyquist frequency, but as indicated by the red plot in Figure 4(b), the limited bandwidth at the output makes it difficult to do so. For this reason, high-speed CTLEs often employ inductive peaking.

The output pole, ω_0, in Figure 4(a) results from the load resistance and capacitance, presenting significant challenges in high-speed CTLE design. The relative magnitudes of this pole and that due to source degeneration lead to different responses and dependencies upon C_S. As shown in Figure 5(a), if $\omega_0 > \omega_p$, then increasing C_S simply shifts the high-pass response to the left. On the other hand, if $\omega_0 < \omega_p$ [Figure 5(b)], then two effects emerge. First, $|H|$ fails to reach its maximum value of $g_m R_D$. Second,

a greater C_1 and hence a lower ω_p reduce the frequency at which the peak occurs. These points encourage us to apply inductive peaking so as to approach the first case.

To raise the boost factor, we can cascade multiple CTLE stages, but at the cost of reduced small-signal bandwidth and greater power consumption. If each stage's bandwidth limitation is approximated by a single pole at $2\pi f_0$, then n identical stages yield a total bandwidth of

$$BW_{tot} = \sqrt{2^{1/n} - 1}\, f_0. \quad (4)$$

For example, two stages lower the bandwidth by 35%. These constraints imply that it is difficult to use more than two CTLE stages, and that the DFE in Figure 2(a) must shoulder the remainder of the equalization.

Pole-Placement Considerations
In the CTLE stage studied previously, we may naturally conclude that the degeneration pole, ω_p, should be placed around the Nyquist frequency. In reality, however, the situation is more complex. With the low available boost factor per stage, the Bode plot of $|H(j\omega)|$ in Figure 4(b) proves inaccurate because ω_z and ω_p are separated by a factor of only 2 to 3. The actual behavior is depicted in Figure 6 and can be quantified as follows. We express $|H(j\omega)|^2$ from (1) as

$$|H(j\omega)|^2 = K^2 \frac{\omega^2 + \omega_z^2}{\omega^2 + \omega_p^2}, \quad (5)$$

where $K = g_m R_D$, and evaluate it at $\omega = \omega_p = (1 + g_m R_S/2)\omega_z$:

$$|H(j\omega_p)|^2 = \frac{K^2}{2}\left[1 + \frac{1}{\left(1 + \frac{g_m R_S}{2}\right)^2}\right]. \quad (6)$$

That is,

$$|H(j\omega_p)| = \frac{K}{\sqrt{2}}\sqrt{1 + \frac{1}{\left(1 + \frac{g_m R_S}{2}\right)^2}}. \quad (7)$$

If the boost factor, $1 + g_m R_S/2$, ranges from 2 to 3, then $|H(j\omega_p)|$ falls between $0.79K$ and $0.74K$, i.e., roughly 2 to 2.5 dB below the maximum value. The key
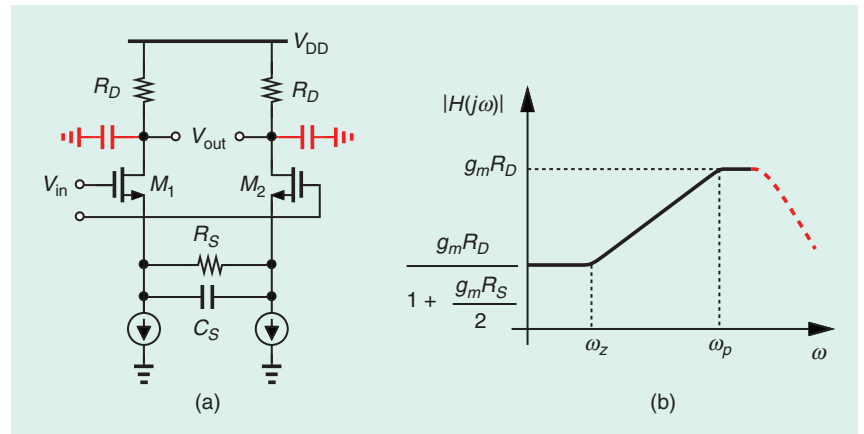
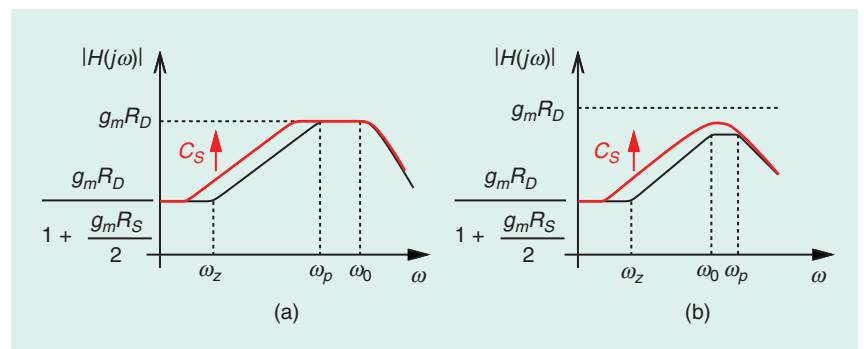**FIGURE 4:** (a) A basic CTLE stage and (b) its approximate response.

FIGURE 5: The CTLE response for (a) $\omega_0 > \omega_p$ and (b) $\omega_0 < \omega_p$.

point here is that, to create maximum boost at f_{Nyq}, the pole frequency should be chosen well below this frequency. For example, to obtain $|H(j2\pi f_{Nyq})| = 0.95K$, (7) indicates that ω_p must be chosen according to

$$\omega_p = \frac{0.312(2\pi f_{Nyq})}{\sqrt{0.95^2 - \dfrac{1}{\left(1 + \dfrac{g_m R_S}{2}\right)^2}}}. \quad (8)$$

For a boost factor of 2 to 3, ω_p ranges from $0.39(2\pi f_{Nyq})$ to $0.35(2\pi f_{Nyq})$, i.e., the pole frequency should be roughly 2.5 to 3 times less than f_{Nyq}.

CTLE Design

CTLE design proceeds in four steps. 1) We place the degeneration pole around one-third of f_{Nyq} and implement the CTLE. 2) We precede the CTLE with the channel and examine the flatness of the cascade response. 3) We study and optimize the eye diagram at the CTLE output. 4) We

FIGURE 6: An illustration of an actual CTLE response.

realize a programmable boost factor. We can then design the DFE and study the performance of the overall equalizer.

We begin the design of our two-stage CTLE with a power budget of 5 mW, leaving the other 5 mW for the DFE. Biased at 2.5 mW, each stage then allows a current of 1.25 mA per transistor. We then select the aspect ratio, W/L, of M_1 and M_2 in Figure 4(a) according to two requirements, namely, the desired transconductance and an acceptable gate-source overdrive voltage. The former plays a role in the boost factor while the latter determines the voltage headroom for the tail current sources and across the drain resistors. According to simulations, a W/L of 10 μm/30 nm gives a g_m of 10 mS and an overdrive of 170 mV, both reasonable values. We then target a boost factor of $1 + g_m R_S/2 = 3$, obtaining $R_S = 400\,\Omega$. We also place ω_p at $2\pi(28\,\text{GHz})/3$ and arrive at a value of 150 fF for C_S. The drain resistors are constrained by the voltage headroom; we select $R_D = 400\,\Omega$ for a voltage drop of 500 mV.

Figure 7(a) depicts the design of the first stage. We load the circuit by an identical stage for now. Figure 7(b) plots the response with $L_D = 0$ and $L_D = 600$ pH, suggesting that inductive peaking raises the boost from 5.4 to 6.2 dB and its corresponding frequency from 15 GHz

to approximately 20 GHz. The dc gain is about unity. The bandwidth falls short of $f_{Nyq} = 28\,\text{GHz}$ and can be increased by lowering R_D but at the cost of dc gain. This tradeoff must eventually be studied when the CTLE-DFE chain is formed.

We now cascade two such stages so as to raise the boost factor [see Figure 8(a)]. As an approximation of the input capacitance of the next stage, two NMOS devices with $W/L = 10\,\mu$m/30 nm are attached to the output nodes. Plotted in Figure 8(b), the overall response exhibits a boost of 14 dB at 25 GHz. Preceding the CTLE with the channel yields the behavior in Figure 8(c) and hence, roughly 8 dB of loss at f_{Nyq}. Unlike the first stage, the second does not see Miller capacitance multiplication, thus achieving a wider bandwidth.

The next step is to study the eye diagrams. Depicted in Figure 9(a) and (b) are the channel and CTLE outputs, respectively. We observe a vertical opening of 250 mV and a horizontal opening of 13 ps.

As mentioned previously, the tradeoff between the dc gain and the boost factor should be examined in a given design. Specifically, does the vertical eye opening in Figure 9(b) increase if the dc gain is raised and the boost is, inevitably, reduced? For example, we can choose $R_S = 300\,\Omega$ and $C_S = 200$ fF. But simulations

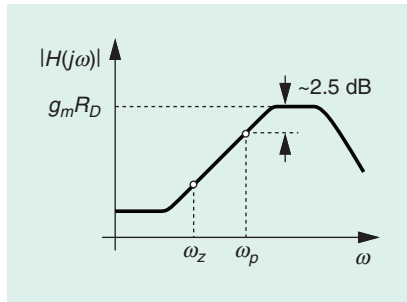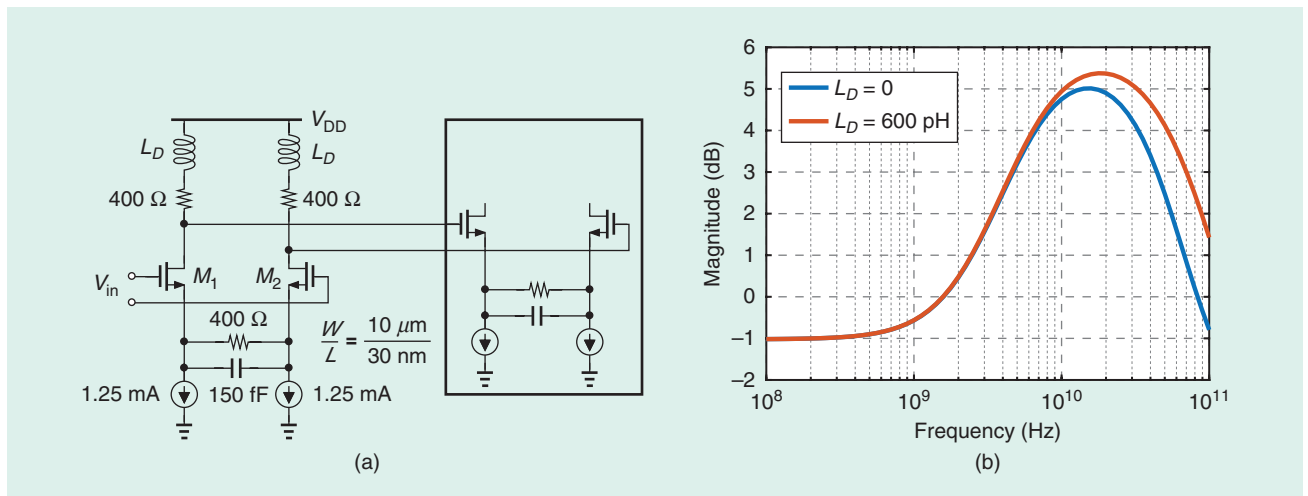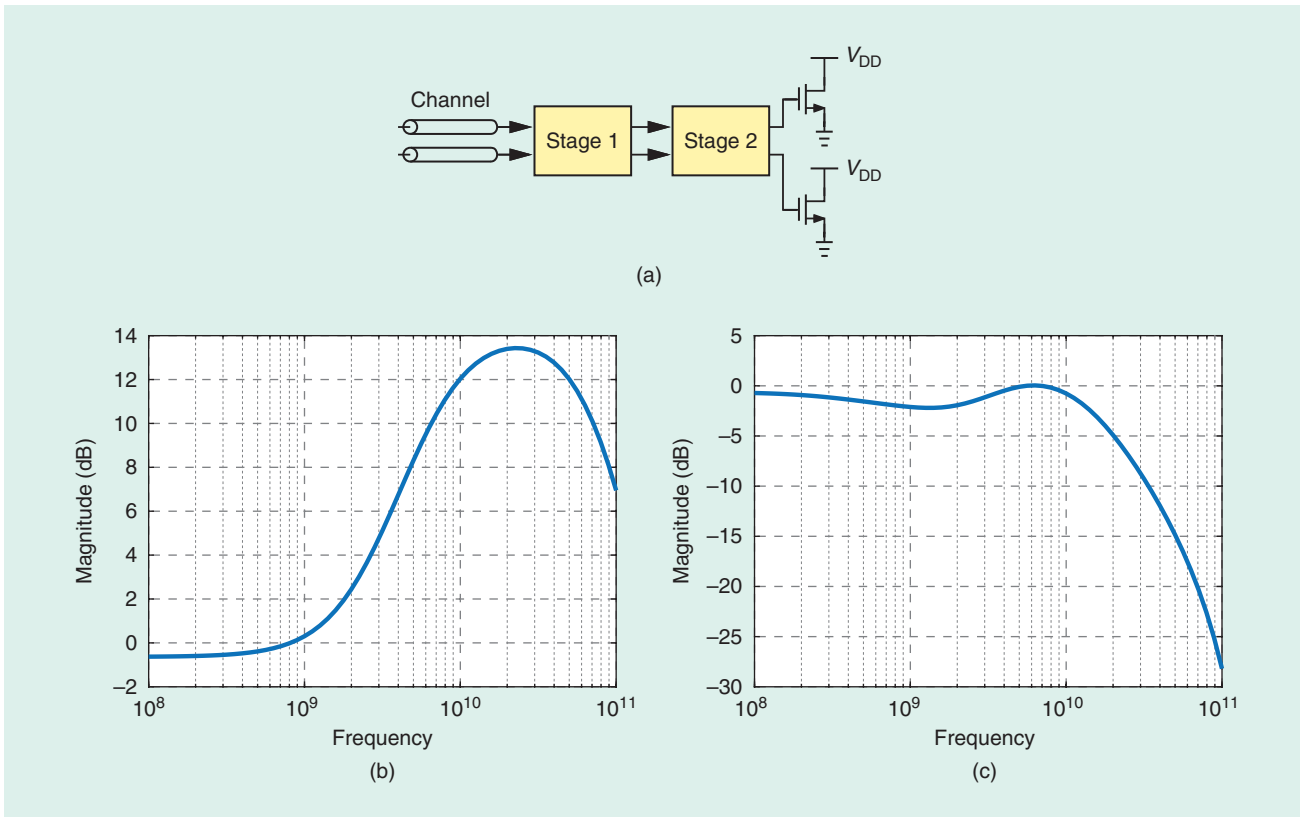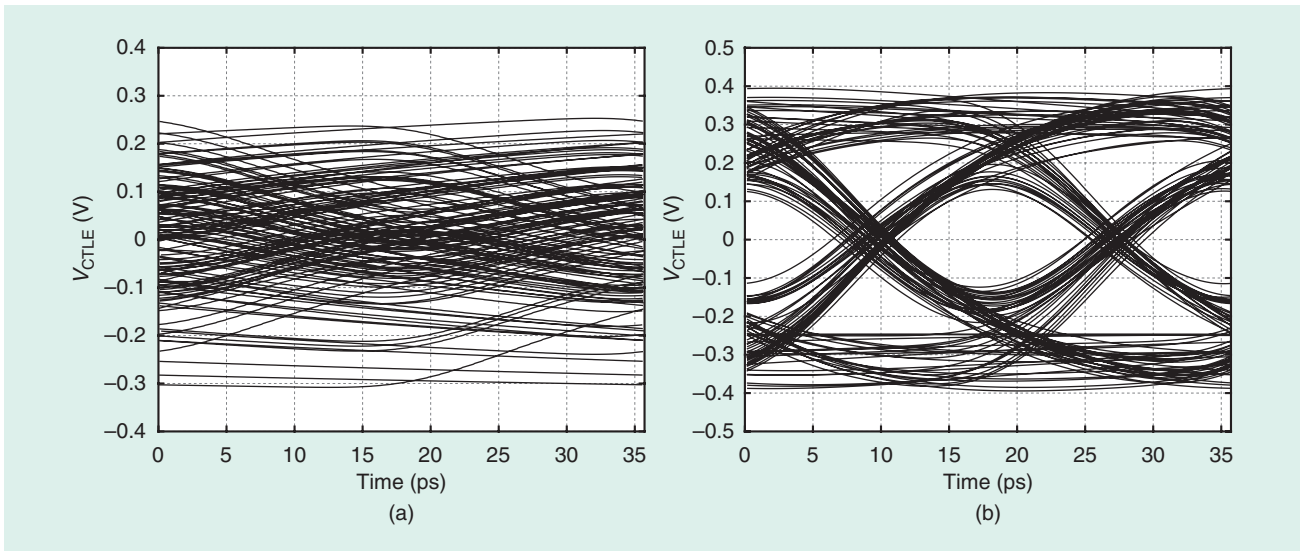**FIGURE 7:** (a) The design of the first CTLE stage and (b) its frequency response.

FIGURE 8: (a) The two-stage CTLE, (b) its frequency response, and (c) the channel-CTLE cascade response.

FIGURE 9: The output eyes of (a) the channel and (b) the CTLE.

reveal that the eye suffers further closure in this case. Conversely, $R_S = 600\,\Omega$ and $C_S = 100$ fF increase the boost factor but do not improve the output eye.

Whether the eye opening depicted in Figure 9(b) is adequate for a BER $< 10^{-12}$ or not is ultimately determined by the DFE design. Our assumption at this point is that the DFE will further improve the eye.

The Need for Programmable Boost
Broadband Rxs must operate properly with different channel responses. The CTLE developed thus far is optimized for a loss of approximately 20 dB at f_{Nyq}, and "overequalizes" the data if the loss is lower. As a result, significant intersymbol interference appears at the CTLE output. For this reason, the boost must be variable. This is typically accomplished by implementing the degeneration capacitors as programmable units. A lower

FIGURE 9: The Best Demo Paper Award was given to two papers at the VLSI 2021: "Energy-Efficient Reliable HZO FeFET Computation-in-Memory with Local Multiply and Global Accumulate Array for Source-Follower and Charge-Sharing Voltage Sensing" by the University of Tokyo, and "A Sub-mW Dual-Engine ML Inference System-on-Chip for Complete End-to-End Face-Analysis at the Edge" by CSEM and ETH Zürich.

online contents and industry systems session. For further information, please visit www.vlsisymposium.org. The Symposium on VLSI Circuits is sponsored by the IEEE Solid-State Circuits Society (SSCS) and the Japan Society of Applied Physics in cooperation with the Institute of Electronics, Information, and Communication Engineers and the IEEE Electron Devices Society (EDS). The Symposium on VLSI Technology is sponsored by EDS and the Japan Society of Applied Physics in cooperation with SSCS.

—*Sugako Otani*
Publicity Chair, Symposium
on VLSI Circuits
SSC

THE ANALOG MIND *(continued from p. 11)*

value pushes the pole to higher frequencies, thereby providing less equalization at f_{Nyq}.

In the second part of this article, we design a DFE and cascade it with the CTLE.

References

[1] S. Gondi and B. Razavi, "Equalization and clock and data recovery techniques for 10-Gb/s CMOS serial-link receivers," *IEEE J. Solid-State Circuits*, vol. 42, no. 9, pp. 1999–2011, Sept. 2007. doi: 10.1109/JSSC.2007.903076.

[2] A. Sheikholeslami, "Equalizer circuit [Circuit Intuitions]," *IEEE Solid-State Circuits Mag.*, vol. 12, no. 1, pp. 6–7, Jan. 2020. doi: 10.1109/MSSC.2019.2952233.

[3] B. Razavi, "The decision-feedback equalizer [A Circuit for All Seasons]," *IEEE Solid-State Circuits Mag.*, vol. 9, no. 4, pp. 13–16, Nov. 2017. doi: 10.1109/MSSC.2017.2745939.

[4] P. Upadhyaya et al., "A fully adaptive 19-to-56Gb/s PAM-4 wireline transceiver with a configurable ADC in 16nm FinFET," in *Proc. IEEE Int. Solid-State Circuits Conf. (ISSCC)*, pp. 108–110. doi: 10.1109/ISSCC.2018.8310207.

[5] T. Ali et al., "A 180mW 56Gb/s DSP-based transceiver for high density IOs in data center switches in 7nm FinFET technology," in *Proc. IEEE Int. Solid-State Circuits Conf. (ISSCC)*, Feb. 2019, pp. 118–120. doi: 10.1109/ISSCC.2019.8662523.

[6] J. Im et al., "A 112-Gb/s PAM-4 long-reach wireline transceiver using a 36-way time-interleaved SAR ADC and inverter-based RX analog front-end in 7nm FinFET," *IEEE J. Solid-State Circuits*, vol. 56, no. 1, pp. 7–18, Jan. 2021. doi: 10.1109/JSSC.2020.3024261.

[7] T. Ali et al., "A 460mW 112Gb/s DSP-based transceiver with 38dB loss compensation for next-generation data centers in 7nm FinFET technology," in *Proc. IEEE Int. Solid-State Circuits Conf. (ISSCC)*, pp. 118–120. doi: 10.1109/ISSCC19947.2020.9062925.

[8] A. Atharav and B. Razavi, "A 56Gb/s 50mW NRZ receiver in 28nm CMOS," in *Proc. IEEE Int. Solid-State Circuits Conf. (ISSCC)*, pp. 192–194. doi: 10.1109/ISSCC42613.2021.9365997.

[9] T. Shibasaki et al., "A 56Gb/s NRZ-electrical 247mW/lane serial-link transceiver in 28nm CMOS," in *Proc. IEEE Int. Solid-State Circuits Conf. (ISSCC)*, pp. 64–66. doi: 10.1109/ISSCC.2016.7417908.

[10] P. J. Peng et al., "A 56Gb/s PAM-4/NRZ transceiver in 40nm CMOS," in *Proc. IEEE Int. Solid-State Circuits Conf. (ISSCC)*, pp. 110–111. doi: 10.1109/ISSCC.2017.7870285.

[11] B. Dehlaghi et al., "A 1.41-pJ/b 56-Gb/s PAM-4 receiver using enhanced transition utilization CDR and genetic adaptation algorithms in 7-nm CMOS," *IEEE Solid-State Circuits Lett.*, vol. 2, no. 11, pp. 248–251, Nov. 2019. doi: 10.1109/LSSC.2019.2938677.

[12] J. Han, N. Sutardja, Y. Lu, and E. Alon, "Design techniques for a 60-Gb/s 288-mW NRZ transceiver with adaptive equalization and baud-rate clock and data recovery in 65-nm CMOS technology," *IEEE J. Solid-State Circuits*, vol. 52, no. 12, pp. 3474–3485, Dec. 2017. doi: 10.1109/JSSC.2017.2740268.

[13] E. Depaoli et al., "A 4.9pJ/b 16-to-64Gb/s PAM-4 VSR transceiver in 28nm FDSOI CMOS," in *Proc. IEEE Int. Solid-State Circuits Conf. (ISSCC)*, pp. 112–114. doi: 10.1109/ISSCC.2018.8310209.

[14] A. Cevrero et al., "A 100Gb/s 1.1pJ/b PAM-4 RX with dual-mode 1-tap PAM-4 / 3-tap NRZ speculative DFE in 14nm CMOS FinFET," in *Proc. IEEE Int. Solid-State Circuits Conf. (ISSCC)*, pp. 112–114. doi: 10.1109/ISSCC.2019.8662495.

[15] A. Roshan-Zamir et al., "A 56-Gb/s PAM-4 receiver with low-overhead techniques for threshold and edge-based DFE FIR- and IIR-tap adaptation in 65-nm CMOS," *IEEE J. Solid-State Circuits*, vol. 54, no. 3, pp. 672–684, Mar. 2019. doi: 10.1109/JSSC.2018.2881278.

[16] A. Manian and B. Razavi, "A 40-Gb/s 14-mW CMOS wireline receiver," *IEEE J. Solid-State Circuits*, vol. 52, no. 9, pp. 2407–2421, Sept. 2017. doi: 10.1109/JSSC.2017.2705913.

[17] P. Mishra et al., "A 112Gb/s ADC-DSP-based PAM-4 transceiver for long-reach applications with >40dB channel loss in 7nm FinFET," in *Proc. IEEE Int. Solid-State Circuits Conf. (ISSCC)*, pp. 138–139. doi: 10.1109/ISSCC42613.2021.9365929.

SSC